Supplementary Information for:

Alteration of the Langerin oligomerization state affects Birbeck Granule formation

Eric Chabrol,[1,2,3] Michel Thépaut,[1,2,3] Colette Dezutter-Dambuyant,[5] Corinne Vivès,[1,2,3] Julien Marcoux,[1,2,3] Richard Kahn,[1,2,3] Jenny Valladeau-Guilemond,[5] Patrice Vachette,[6] Dominique Durand,[6,*] and Franck Fieschi,[1,2,3,4,*].

[1]University Grenoble Alpes, IBS, Grenoble, France; [2]CNRS and [3]CEA, UMR 5075, Grenoble France; [4]Institut Universitaire de France, Paris, France; [5]Centre Léon Bérard-UMR INSERM 1052-CNRS 5286, Centre de recherche en Cancérologie de Lyon, Lyon, France; [6]Institut de Biologie Intégrative de la Cellule, CEA, CNRS, Université Paris Sud, Gif sur Yvette, France

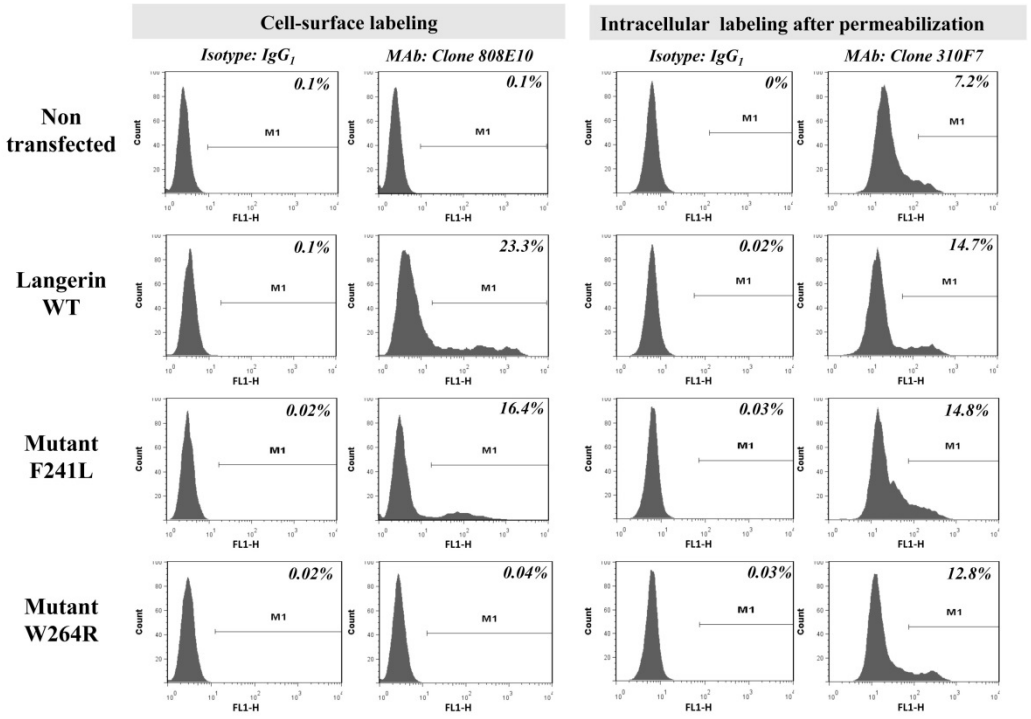

Figure S1. FACS analysis of COP5 cells transfected or not with: langerin$_{WT}$, langerin$_{F241L}$ and langerin$_{W264R}$. Anti-langerin mAb (clone 808E10) was used to detect langerin on cell surface and mAb clone 310F7 for intracellular labeling after permeabilization with 0.3% saponin in 2% BSA. The marker bar (M1) corresponds to the fraction of positive cells in the total cell population (%).

Supplemental Table S1.

Table S1: Lg-CRD$_{F241L}$ data collection and structure refinement statistics.

Data collection statistics	
Wavelength (Å)	0.933
Space group	$P4_2$
Unit cell parameters (Å)	a = b = 79.96; c = 90.42
Resolution (Å)	50- 1.4 (1.48-1.4) [a]
Measured reflections	834069 (130176)
Unique reflections	111136 (17644)
Completeness (%)	99.2 (98)
I/σ (I)	24.88 (4.7)
R_{merge} [b] (%)	5.3 (32.7)
Structure refinement statistics	
Resolution (Å)	19.5-1.4
Refinement factors	
Used reflections/free (%)	105603/ 4.9752
R_{cryst} [c]	0.1775
R_{free} [c]	0.2186
Rmsd from ideality	
Bond lengths (Å)	0.009
Bond angles (deg)	1.280
Average B-factor (Å^2)	14.88

[a] Values in parentheses are for the highest resolution shell. [b] $R_{merge} = \sum_h\sum_m| I_m(h) - \langle I(h)\rangle | / \sum_h\sum_m I_m(h)$. [c] $R_{cryst} = \sum||F_0| - |F_c|| / \sum|F_0|$, and $R_{free} = R_{cryst}$ calculated with 5% of F_0 set aside before refinement.

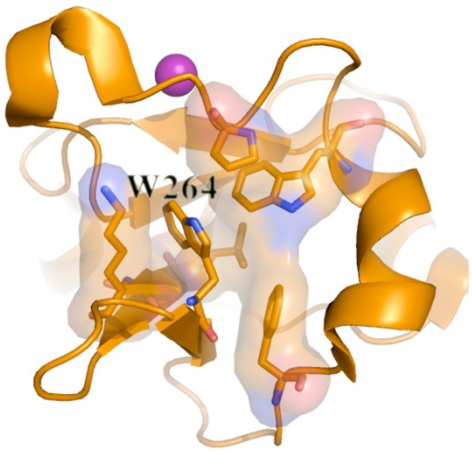

Figure S2. Focus on W264 hydrophobic cluster in Lg-CRD$_{WT}$ structure.

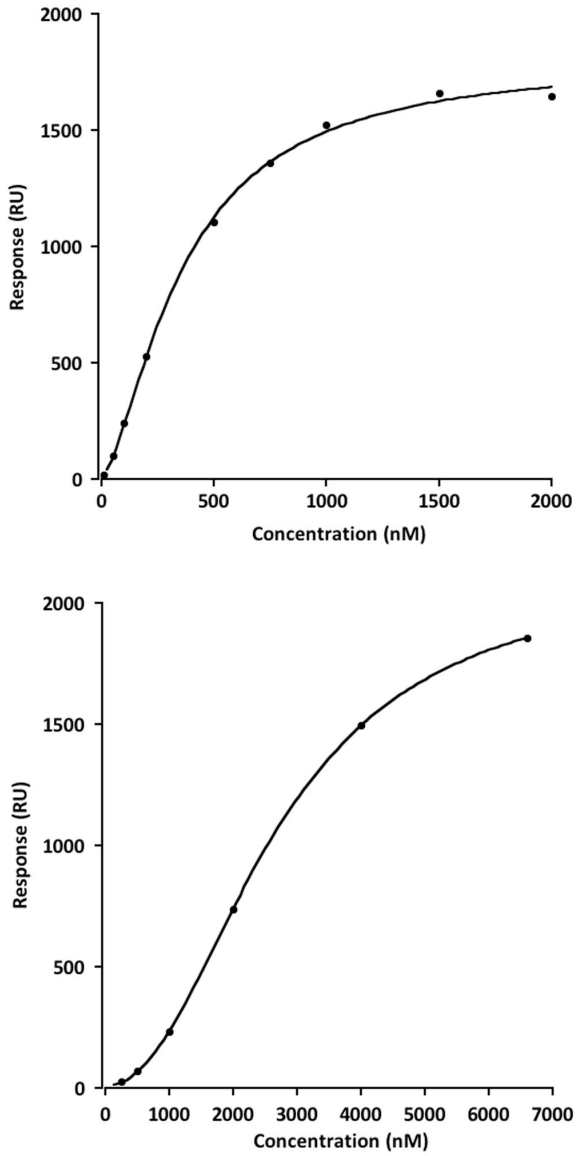

Figure S3. Binding curves for Lg-ECD$_{WT}$ (top) and Lg-ECD$_{F241L}$ (bottom) onto gp120 functionalized surfaces. Due to the complexity of the multivalent interaction, involving up to three binding sites on the langerin side and multiple ligand exposed on the heavily glycosylated gp120 side, it is not possible to determine real K_d value using classical fit for 1:1 interaction. Apparent binding efficacy is thus evaluated using EC_{50} determination (effective concentration). Data are fitted using 4 parameters logistic model (equation 1 below). R_{eq} represents the binding response, R_{lo} the lower response, R_{hi} the upper asymptote (the R_{max}), b is the slope factor and c, the inflexion point, is considered as the relative EC_{50}. Absolute EC_{50} is determined using equation 2.

$$\mathrm{R}\,eq = \frac{R_{lo} - R_{hi}}{1 + \left(\frac{Conc}{c}\right)^{b}} + R_{hi} \qquad (1) \qquad , \qquad EC_{50} = c \cdot \left(\frac{R_{hi} - R_{lo}}{R_{hi} - 50} - 1\right)^{\frac{1}{b}} \qquad (2)$$

For Lg-ECD$_{WT}$ and Lg-ECD$_{F241L}$, EC_{50} of 0.36 µM and 2.67 µM were obtained respectively (a ratio of 7.4 from WT to mutant).

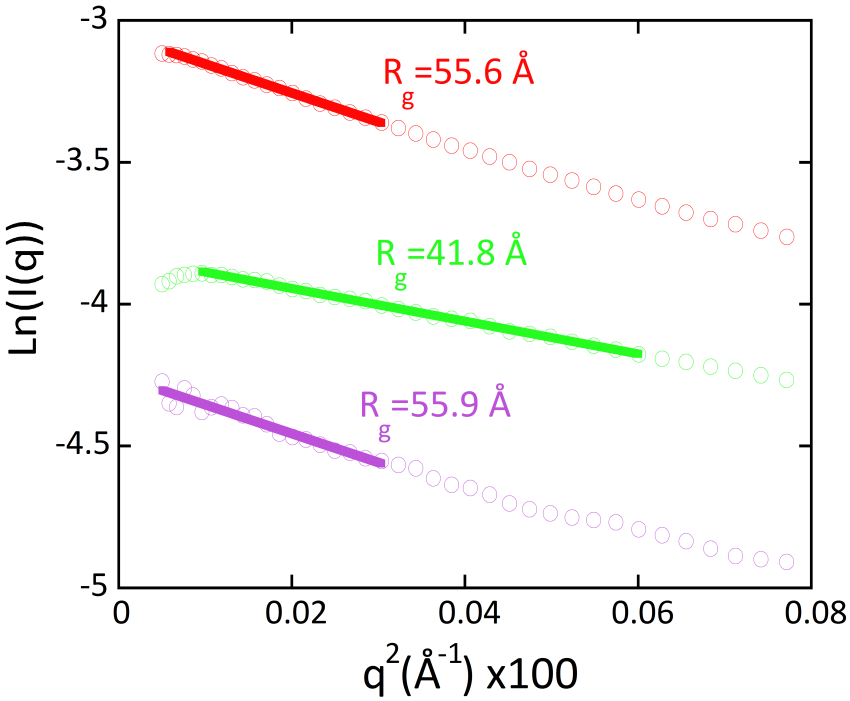

Figure S4. Guinier plots. The three Guinier plots are shown for the Lg ECD_{WT},(red), Lg ECD_{F241L} trimer (violet) and Lg ECD_{F241L} dimer (green). Error bars are smaller than the symbols.

WT trimer modelling attempt.

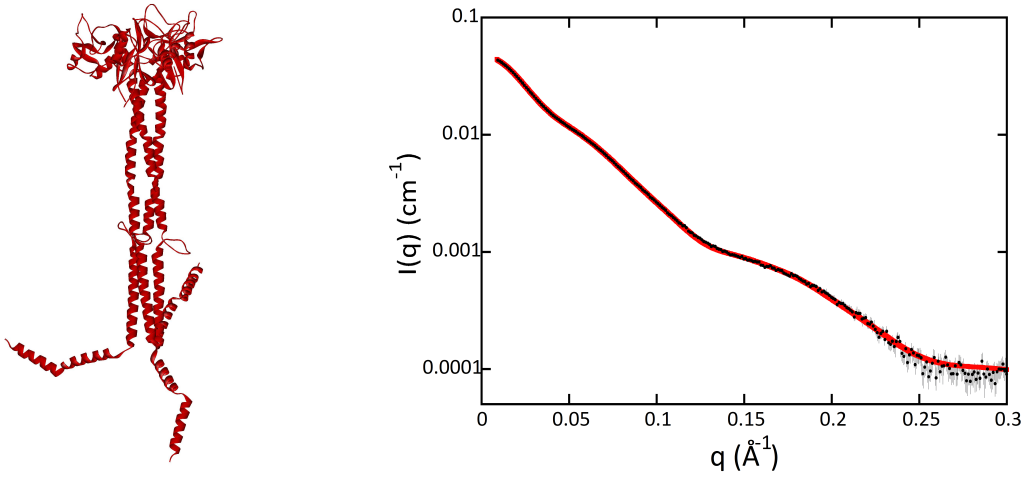

Figure S5. Left, model of Langerin ECD_{WT} trimer. Right, SAXS experimental data of Lg ECD_{WT} (black dots with associated error bars in grey) and calculated curve from the model shown on the left (red line). For q<0.18 $Å^{-1}$ error bars are smaller than the size of the black dots.

First, the N-terminal stretch (68-95) presents a weak or altogether absence of chain pairing (Logicoil prediction) but is still predicted to be mainly helical. We thus model this region by a succession of two helices that may change mutual position during modelling. Second, all approaches point towards the existence of disorder in the region 140-150. We modelled this as follows: we first moved the distal coiled-coil fragment 107-138 together with the N-terminal stretch up towards the C-terminal fragment so as to shorten the neck as required by the p(r) profile. We modelled the connecting loops 138-150 using Modloop (1). We then used rigid-body modelling as implemented in SASREF to determine the arrangement of all three N-terminal stretches – each one comprising two helices - with respect to the rest of the molecule so as to fit the data. Several runs yield a satisfactory fit (χ=1.48) to the data with resulting models in which at least one N-tail is folded back towards the coiled-coil as shown in Figure S1. This model is a proposal compatible with our data and the results of sequence analyses.

1. Fiser, A., and.Sali. 2003. ModLoop: automated modeling of loops in protein structures. Bioinformatics. 19:2500-2501.

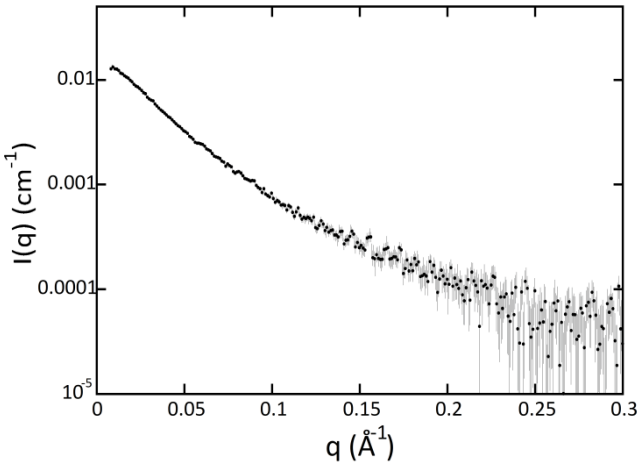

Figure S6. SAXS experimental data of the trimer of Lg ECD_{F241L} (black dots with associated error bars in grey).